Bioactive Materials xxx (xxxx) xxx

Contents lists available at ScienceDirect

Bioactive Materials

journal homepage: www.keaipublishing.com/en/journals/bioactive-materials

A hierarchical bilayer architecture for complex tissue regeneration

Min Yu [a,b,1], Dan Luo [c,1], Jing Qiao [d,1], Jiusi Guo [e], Danqing He [a], Shanshan Jin [a], Lin Tang [b], Yu Wang [a], Xin Shi [f], Jing Mao [f], Shengjie Cui [a], Yu Fu [g], Zixin Li [a], Dawei Liu [a], Ting Zhang [a], Chi Zhang [c], Zhou Li [c,**], Yongsheng Zhou [b,***], Yan Liu [a,*]

[a] *Laboratory of Biomimetic Nanomaterials, Department of Orthodontics, Peking University School and Hospital of Stomatology & National Center of Stomatology & National Clinical Research Center for Oral Diseases & National Engineering Laboratory for Digital and Material Technology of Stomatology & Beijing Key Laboratory of Digital Stomatology & Research Center of Engineering and Technology for Computerized Dentistry Ministry of Health & NMPA Key Laboratory for Dental Materials, Beijing, 100081, China*

[b] *Department of Prosthodontics, Peking University School and Hospital of Stomatology & National Center of Stomatology & National Clinical Research Center for Oral Diseases & National Engineering Laboratory for Digital and Material Technology of Stomatology & Beijing Key Laboratory of Digital Stomatology & Research Center of Engineering and Technology for Computerized Dentistry Ministry of Health & NMPA Key Laboratory for Dental Materials, Beijing, 100081, China*

[c] *CAS Center for Excellence in Nanoscience, Beijing Key Laboratory of Micro-nano Energy and Sensor, Beijing Institute of Nanoenergy and Nanosystems, Chinese Academy of Sciences, Beijing, 101400, China*

[d] *Department of Periodontology, The First Clinical Division, Peking University School and Hospital of Stomatology, Beijing, 100034, China*

[e] *State Key Laboratory of Oral Diseases, National Clinical Research Center for Oral Diseases, West China Hospital of Stomatology, Sichuan University, Chengdu, 610041, China*

[f] *Center of Stomatology, Tongji Hospital, Tongji Medical College, Huazhong University of Science and Technology, Wuhan, 430030, China*

[g] *Fourth Division, Peking University Hospital of Stomatology, Beijing, 100025, China*

ARTICLE INFO

Keywords:
Biomimetic design
Biphasic scaffold
Mineralized collagen
Micropatterned arrays
Periodontium regeneration

ABSTRACT

Engineering a complete, physiologically functional, periodontal complex structure remains a great clinical challenge due to the highly hierarchical architecture of the periodontium and coordinated regulation of multiple growth factors required to induce stem cell multilineage differentiation. Using biomimetic self-assembly and microstamping techniques, we construct a hierarchical bilayer architecture consisting of intrafibrillarly mineralized collagen resembling bone and cementum, and unmineralized parallel-aligned fibrils mimicking periodontal ligament. The prepared biphasic scaffold possesses unique micro/nano structure, differential mechanical properties, and growth factor-rich microenvironment between the two phases, realizing a perfect simulation of natural periodontal hard/soft tissue interface. The interconnected porous hard compartment with a Young's modulus of 1409.00 ± 160.83 MPa could induce cross-arrangement and osteogenic differentiation of stem cells *in vitro*, whereas the micropatterned soft compartment with a Young's modulus of 42.62 ± 4.58 MPa containing abundant endogenous growth factors, could guide parallel arrangement and fibrogenic differentiation of stem cells *in vitro*. After implantation in critical-sized complete periodontal tissue defect, the biomimetic bilayer architecture potently reconstructs native periodontium with the insertion of periodontal ligament fibers into newly formed cementum and alveolar bone by recruiting host mesenchymal stem cells and activating the transforming growth factor beta 1/Smad3 signaling pathway. Taken together, integration of self-assembly and microstamping strategies could successfully fabricate a hierarchical bilayer architecture, which exhibits great potential for recruiting and regulating host stem cells to promote synergistic regeneration of hard/soft tissues.

Peer review under responsibility of KeAi Communications Co., Ltd.

* Corresponding author. Peking University School and Hospital of Stomatology, 22nd Zhongguancun South Ave, Haidian District, Beijing, 100081, China.

** Corresponding author. Beijing Institute of Nanoenergy and Nanosystems, Chinese Academy of Sciences, No. 8 Yard, Yangyandong 1st Road, Yanqi Economic Development Zone, Huairou District, Beijing, 101400, China.

*** Corresponding author. Peking University School and Hospital of Stomatology, 22nd Zhongguancun South Ave, Haidian District, Beijing, 100081, China.

E-mail addresses: zli@binn.cas.cn (Z. Li), kqzhouysh@hsc.pku.edu.cn (Y. Zhou), orthoyan@bjmu.edu.cn (Y. Liu).

[1] These authors contributed equally.

https://doi.org/10.1016/j.bioactmat.2021.08.024

Received 25 May 2021; Received in revised form 20 August 2021; Accepted 20 August 2021

1. Introduction

The periodontium, a hierarchically organized organ comprising intercalated hard mineralized (bone and cementum) and soft unmineralized (periodontal ligament) tissues, provides mechanical and physical support to the teeth. As one of three major oral diseases listed by the World Health Organization, periodontitis caused by plaque microorganisms not only destroys the periodontal tissues and eventually leads to tooth loss but also impairs general health [1]. Regeneration of periodontal tissues remains challenging because it is difficult to reconstruct the sophisticated mineralized/unmineralized hierarchical architecture of periodontal tissue [2]. Novel tissue engineering strategies that combine biodegradable scaffolds with growth factors exhibit great potential in regenerative medicine [3]. Growth factor delivery and the physiological environment provided by biomimetic scaffolds can contribute to the regulation of periodontal and mesenchymal stem cell migration, proliferation, differentiation, chemotaxis, and extracellular matrix (ECM) production, giving rise to a promising therapeutic approach for periodontal regeneration [4].

A variety of scaffolds loaded with biological factors have been developed, e.g., a supramolecular hydrogel Nap-Phe-Phe-Tyr-OH coassembled with stromal cell-derived factor 1 and bone morphogenetic protein 2 (BMP2) was found to synchronously and continuously release the two bioactive factors to effectively promote reconstruction of periodontal bone tissue [5]. However, in the majority of previous studies, only monophasic scaffolds were fabricated, thus limiting their application to single tissue regeneration. It is not possible to regenerate complex multiphase tissues, such as periodontal tissue, using a simple monophasic architecture [6,7]. Multiphasic constructs, recapitulating the native periodontium architecture with distinctly different physical and chemical properties, have been advocated for periodontal tissue regeneration. Based on the principle of guided tissue regeneration, multiphasic scaffolds have been fabricated to simulate soft/hard tissue interfaces, which include a semi-rigid polylactide-co-glycolide acid and calcium phosphate-based bilayered biomaterial [8], a biomimetic hybrid bilayer of polycaprolactone and poly (glycolic acid) [9], and a triphasic hydrogel scaffold consisting of chitin-poly (lactic-co-glycolic acid)/nanobioactive glass ceramic/cementum protein [10]. Recently, 3D rapid prototyped scaffolds could tailor mechanical, mass transport and architectural features as well as with integrated functionalities for complex tissue regeneration [11–13]. Although previously reported multiphasic scaffolds mimicking the differential structure and mechanical characteristics of periodontal tissue could yield a periodontium-like structure to a certain degree, complete, functional periodontium regeneration (including both hard and soft tissues) remains challenging. In addition, there have been little reports mentioned the simulation of the hierarchical micro/nano structure and unique growth factor microenvironment of the periodontium; debate remains regarding the mechanism underlying multilineage differentiation of stem cells to form soft and hard tissues.

Periodontal tissue regeneration should meet the following three prerequisites: (i) construction of a mineralized/unmineralized diphasic scaffold with distinct mechanical properties, (ii) fabrication of a hierarchical micro/nano topology to simulate the natural periodontium structure, and (iii) provision of differentiated growth factors to recruit host mesenchymal stem cells and induce multilineage differentiation. Recently, we successfully developed an intrafibrillarly mineralized collagen (IMC) scaffold exhibiting excellent mechanical properties, biocompatibility, and biodegradability [14–16]. This biomimetic IMC scaffold was shown to regulate and determine the fate of periodontal ligament stem cells (PDLSCs) and bone marrow stromal cells, and exhibited excellent bone regeneration potential [17–19]. However, only achieving bone regeneration is insufficient to support the reconstruction of periodontal tissue, and regeneration of the periodontal ligament, an unmineralized soft tissue, is equally important. Concentrated growth factor (CGF), belonging to a novel generation of platelet concentrate products, can potentially participate in the regeneration of soft tissue, which is rich in various endogenous growth factors, leukocytes, and $CD34^+$ cells within a fibrin network [20]. With the help of the fibrin network, CGF is thought to coagulate into an unmineralized soft scaffold for periodontal ligament regeneration. Moreover, abundant endogenous growth factors can further regulate cell fate [21–23]. High levels of endogenous growth factors, such as platelet-derived growth factor-BB (PDGF-BB), transforming growth factor beta 1 (TGF-β1), vascular endothelial growth factor (VEGF), insulin-like growth factor 1 (IGF-1), and basic fibroblast growth factor (bFGF), are involved in soft and hard tissue regeneration [24]. In the present study, a biomimetic bilayer architecture consisting of IMC scaffold (resembling bone and cementum) and unmineralized collagenized-CGF fibrils arranged in parallel (mimicking periodontal ligament) was synthesized via the integration of self-assembly and microstamping techniques. This hierarchical architecture contained a stable and distinct diphase interface. The hard tissue compartment with interconnected pores could induce an osteoblast-like arrangement and osteogenic differentiation of PDLSCs. Meanwhile, the soft tissue compartment with micropatterned CGF fibrils could release endogenous growth factors, such as TGF-β1 and VEGF, to orient PDLSCs into a fibroblast-like arrangement and guide fibrogenic differentiation. At 8 weeks after implantation, the biomimetic bilayer architecture potently reconstructed native periodontium by recruiting host mesenchymal stem cells and activating the TGF-β1/Smad3 pathway.

2. Materials and methods

2.1. Fabrication of hierarchical CGF/IMC bilayer architecture

Parallel-aligned CGF arrays were produced using a microstamping technique. Briefly, 8 mL of blood sample was separately drawn from nine volunteers by venipuncture of the antecubital vein, collected into sterile Vacuette tubes with white cap (Greiner Bio-One, GmbH, Austria) without anticoagulant solutions, and immediately centrifuged (Medifuge, Silfradentsrl, Sofia, Italy) in a built-in program. The protocols were approved by Ethics Committee of Peking University School of Stomatology (PKUSSIRB-201951179). Then, the upper liquid phase and the lower red blood cell phase were formed. After the top 2 mL of the upper liquid phase was removed, CGF was collected, including the remaining upper liquid phase and the top 3 mm of red blood cell phase (Fig. S1). After being aspirated and mixed evenly, CGF was mixed with type I collagen (Corning, 0.5 mg mL^{-1}) at a 1:2 v/v ratio, and the mixture was coated onto microstamping models with width interval of 50 μm (Fig. S2). After coagulation for 30 min at room temperature, stable and parallel-aligned CGF arrays were obtained. To verify the stability of parallel-aligned CGF arrays, pure CGF and collagen-reinforced CGF were immersed into the culture medium for 2 days, and then observed by a Zeiss light microscope.

The porous IMC scaffold was fabricated by a biomimetic self-assembly approach as previously described [14–16]. Briefly, type I tropocollagen solution (Corning) was reconstituted in a dialysis flask (3500 Da), immersed in a mineralization solution at 37 °C for 7 days. Then, the mineralized collagen was formed a just-castable suspension, poured into the molds, frozen overnight at −40 °C and lyophilized to form sponge-like porous scaffolds.

The parallel-aligned CGF arrays were imprinted onto the porous IMC layer to achieve combination and compatibility between the IMC phase and the CGF phase, quickly frozen in liquid nitrogen and lyophilized to obtain the CGF/IMC bilayer scaffold. To enhance stabilization, the CGF/IMC bilayer scaffolds were cross-linked with 0.3 M 1-ethyl-3-(3-dimethylaminopropyl)-carbodiimide and 0.06 M *N*-hydroxysuccinimide for 4 h and rinsed alternately in 1 wt% glycine solution and deionized water for three times.

2.2. Scanning electron microscopy (SEM)

The microstructure of the CGF/IMC bilayer scaffold was observed using SEM (Hitachi S-4800, Japan). The samples were dehydrated in a graded series of ethanol (50 %–100%) and critical-point dried, and then sputter-coated with gold for 2 min at 20 mA.

2.3. Laser scanning confocal microscope (LSM)

The microstructure of the CGF layer and the IMC layer was observed by LSM (LSM-710, Zeiss). Before the process of microstamping, quantum dots with autofluorescence were mixed with collagen-reinforced CGF. The IMC layer was incubated with the primary antibodies against COL-1 (Abcam) at 1:200 dilution for 2 h and tetramethylrhodamine isothiocyanate-conjugated secondary antibodies (TRITC, Zhongshan Golden Bridge Biotechnology) for 1 h. After washing thrice, the sample was mounted with mounting media not containing 4′,6-diamidino-2-phenyl-indole (DAPI) and viewed by LSM-710.

2.4. Atomic force microscopy (AFM)

The nanomechanical properties of the CGF layer and the IMC layer were tested using AFM (Dimension Icon, Bruker, USA). Under ambient condition (room temperature), the CGF layer and the IMC layer were separately assembled onto freshly cleaved mica, and at least three scanning areas were performed in each layer. The obtained property maps with 512 × 512 pixels were analyzed using NanoScope 18 software. Data for statistical analysis was collected from at least three independent samples.

2.5. Transmission electron microscopy (TEM)

The nanostructure of IMC and CGF was characterized by TEM (JEOL JEM-1011). The samples were embedded in epoxy resin, sectioned with an ultramicrotome, and collected on TEM grids. Before observation, CGF fibrils were stained with uranyl acetate and lead citrate.

2.6. Thermogravimetric analysis and differential scanning calorimetry (TGA/DSC)

The mineral content in IMC was determined by TGA/DSC (TGA/DSC 3+, Mettler Toledo) in the temperature range from room temperature to 800 °C at a heating rate of 10 °C/min in nitrogen. The lyophilized IMC and pure collagen scaffolds were cut into small pieces and about 5 mg of samples were used for measurement.

2.7. Growth factor expression of the CGF/IMC bilayer architecture

The expression of two important growth factors in the CGF/IMC bilayers was detected by immunofluorescent staining of the CGF layer and cross-sections of the CGF/IMC bilayers. After fixed by 4% paraformaldehyde for 30 min, the samples were washed thrice, and blocked with bovine serum albumin (5% w/v) for 1 h. Then, the samples were incubated with the primary antibodies against TGF-β1 (Abcam), PDGF-BB (Affinity) and VEGF (Abcam) at a 1:200 dilution for 2 h. Fluorescein isothiocyanate-conjugated secondary antibodies (FITC, Zhongshan Golden Bridge Biotechnology) were used to bind primary antibodies for 1 h at room temperature. After washing thrice, the samples were mounted with mounting media not containing DAPI and viewed by LSM-710.

Further, the release profile of TGF-β1 and VEGF from the CGF/IMC bilayers was investigated *in vitro*. Three CGF/IMC bilayer scaffolds were separately incubated with 2 mL culture medium (Dulbecco's modified Eagle medium with 1% penicillin/streptomycin) at 37 °C for 14 days. The supernatant was collected at 1, 3, 5, 7, 9, and 14 days, and an equal volume of fresh medium was immediately supplemented. All collected supernatants were quantified using enzyme-linked immunosorbent assay kits (R&D systems).

2.8. Human PDLSC isolation and identification

Isolation of human primary PDLSCs was performed as previously described [42]. In brief, periodontal ligament was scratched from root surface and digested in a mixture of 4 mg mL^{-1} dispase II (Solarbio) and 3 mg mL^{-1} type I collagenase (Sigma) for 1 h at 37 °C. Then, the single-cell suspensions were used for cell culture and the obtained PDLSCs were used at the fourth passage. All protocols were approved by Ethical Committee of Peking University School of Stomatology (PKUSSIRB-201951179). To identify multidirectional differentiation ability of obtained PDLSCs, cells were cultured in osteogenic differentiation condition medium for 7 days and 14 days, and stained with alkaline phosphatase (ALP) and Alizarin Red. Cells were cultured in adipogenic differentiation condition medium for 14 days, and stained with Oil Red O.

2.9. Cell counting kit-8 assay

Biocompatibility of the CGF/IMC scaffolds was determined using the Cell Counting Kit-8 assay (CCK-8). Human PDLSCs identified were seeded on the CGF/IMC scaffolds on days 1, 3, 5. Quantification was performed with a microplate reader of optical density (OD) value at 450 nm according to the manufacturer's protocol.

2.10. Immunofluorescent staining

To investigate the respective biological effects between the CGF phase and the IMC phase, the binary CGF/IMC scaffolds were divided into monophasic, two-dimensional slices. Human PDLSCs were seeded separately onto the CGF and IMC slices for 1 day, and cell morphology was evaluated by immunofluorescent staining. The samples were fixed in 4% paraformaldehyde for 30 min, permeabilized with 0.25% Triton-X for 15 min, and blocked by bovine serum albumin (5% w/v) for 1 h. Subsequently, cells were stained with Alexa Fluor 488 Phalloidin (F-actin) for 1 h. After washing with phosphate buffered saline (PBS), the cells were mounted with mounting media containing DAPI and viewed by LSM 710.

2.11. Quantitative real-time polymerase chain reaction (RT-PCR)

To investigate cell multilineage differentiation on the CGF/IMC biphasic scaffold *in vitro*, human PDLSCs were cultured onto the CGF and the IMC slices with fibrogenic differentiation conditioned medium (regular medium supplemented with 100 ng mL^{-1} recombinant human connective tissue growth factor and 50 μg mL^{-1} ascorbic acid) for 7 days, and osteogenic differentiation conditioned medium (regular medium supplemented with 10^{-7} M dexamethasone, 10 mM β-glycerophosphate and 0.05 mM ascorbic acid 2-phosphates) for 14 days separately. Quantitative RT-PCR was applied to evaluate the expression of fibrogenic differentiation gene markers (*Postn* and *elastin*), osteogenic differentiation gene markers (*Runx2* and *OPN*). Total RNA was extracted with Trizol reagent (Invitrogen) and synthesis of cDNA was performed using SuperScript III One-Step RT-PCR System with Platinum Taq High Fidelity (Invitrogen). Quantitative RT-PCR was performed on a 7500HT Fast Real Time PCR using SYBR Green (Invitrogen). The primers synthesized were as follows:

Human-*GAPDH* GGAGCGAGATCCCTCCAAAAT and GGCTGTTGTC ATACTTCTCATGG
Human-*Postn* TGGAGAAAGGGtAGTAAGCAAGG and TTCAAGTAGG CTGAGGAAGGTG
Human-*Elastin* AAAGCAGCAGCAAAGTTCGG and ACCTGGGACAAC TGGAATCC

Human-*Runx2* CACTGGCGCTGCAACAAGA and CATTCCGGAGCTC AGCAGAATAA
Human-*OPN* CAGTTGTCCCCACAGTAGACAC and GTGATGTCCTCG TCTGTGCATC

2.12. Western blotting

Western blotting was performed according to our previously published protocols [25]. Briefly, Cell lysate proteins were harvested by RIPA Buffer (Thermo Fisher Scientific), separated by 10% SDS–polyacrylamide gel electrophoresis, and then transferred to polyvinylidene difluoride membranes and blocked in 5% nonfat milk. The membranes were separately probed with corresponding primary antibodies against GAPDH (1:1000, Proteintech), POSTN (1:1000, Abcam), ALP (1:500, Affinity), SP7 (1:1000, Abcam), TGF-β1 (1:1000, Abcam), Smad3 (1:1000, CST) and p-Smad3 (1:1000, CST) overnight at 4 °C. Membranes were washed three times in TBS with 0.1% Tween-20, incubated with an HRP-conjugated secondary antibody for 1 h, and imaged by an Odyssey® Imaging System. Quantitative analysis was performed by ImageJ software.

2.13. Rat complete periodontal defect model

Forty male Sprague-Dawley rats (200–220 g, 8 weeks old) were randomly divided into four groups including the Blank, CGF, CGF–DBBM and CGF/IMC groups ($n = 10$). After anaesthetized and disinfected, the buccal alveolar bone, periodontal ligament and root surface of the mandibular first molar were removed with round burs and the periodontal defect (5 mm × 4 mm × 1 mm) was created. After 4 or 8 weeks, rats were sacrificed by over-anesthesia, and the right mandibles were obtained and fixed with 10% formalin. All animal procedures were approved by Peking University Institutional Animal Care and Use Committee (No. LA2019072). According to periodontal fenestration defect models in previous studies [43], we removed all the buccal alveolar bone, periodontal ligament, and cementum, and the root surface could be seen. For Blank group, the periodontal defect area was filled without any scaffolds and covered with Bio-Gide® membrane. For experimental groups, the periodontal defect region was filled with CGF, CGF–DBBM and CGF/IMC scaffolds respectively, and covered with Bio-Gide® membrane.

2.14. Subcutaneous ectopic regeneration model in immunodeficient mice

To further confirm the functional role of the CGF/IMC biphasic scaffold in the recruitment and multi-lineage differentiation of host MSCs, the CGF–DBBM and the CGF/IMC scaffolds were implanted into subcutaneous pockets on the back of immunodeficient mice (20–25 g, 6–8 weeks old). After 8 weeks of implantation, all scaffolds were obtained and fixed with 4% paraformaldehyde for histochemical staining and SEM observations.

2.15. Microcomputed tomographic (micro-CT) analysis

All fixed samples were scanned with a micro-CT system (Skyscan 1174, Bruker, Belgium) at 53 kV and 810 μA. The NRecon and CTvox software were used for three-dimensional image reconstruction. The region of interests of entire alveolar bone defect area was selected semiautomatically, and the bone volume and thickness of the newly formed alveolar bone were measured by the CTAn software (Bruker).

2.16. Histological staining assessment

The samples were demineralized in 10% ethylenediaminetetraacetic acid and embedded in paraffin. Serial 5 μm-thick horizontal sections were prepared and stained with HE and Masson's trichrome staining according to standard procedures. The formation and organization of regenerated tissues were observed using a Zeiss light microscope and evaluated from at least 5 randomly selected fields from each specimen with Image Pro Plus software. New alveolar bone formation was defined as the bone island observed within defect area. Percentage of new bone formation was calculated by dividing the area of new bone with the area of the defect. New cementum was defined as the mineralized tissue formed on the denuded root surface with collagen fibers inserted. The percentage of new cementum covering the denuded root surface was calculated by dividing the length of root surface with new cementum with the length of the whole denuded root surface. The percentage of new periodontal ligament was calculated by dividing the length of root surface with functional periodontal ligament attachment with the length of the whole denuded root surface.

For immunofluorescent staining, selected sections were subjected to antigen retrieval using 0.125% trypsin and 20 μg mL^{-1} proteinase K at 37 °C for 30 min, blocked with 5% bovine serum albumin for 1 h, and subsequently incubated with primary antibodies against CD90 (BD Pharmingen), CD105 (Abcam) and TGF-β1 (Abcam) at 1:200 dilution overnight at 4 °C. Next, FITC and TRITC secondary antibodies were simultaneously used to bind primary antibodies for 1 h. After washing thoroughly with PBS, the samples were mounted with mounting media containing DAPI and viewed by LSM-710. For immunohistochemistry staining, selected sections were deparaffinized, blocked and incubated with primary antibodies against CD146 (Abcam), STRO-1 (eBioscience), OCN (Abcam), BMP2 (Abcam), COL-1 (Abcam), VEGFR-1 (Abcam), TGF-β1 (Abcam) and Smad3 (Abcam) at 1:200 dilution overnight at 4 °C. Following by washing, the samples were incubated with horseradish peroxidase-conjugated secondary antibodies (Zhongshan Golden Bridge Biotechnology). Each group was composed of more than 3 slides and observed under a Zeiss light microscope.

2.17. Statistical analysis

All semi-quantitative data were obtained from at least three samples and/or three independent experiments and expressed as mean ± standard deviation. Statistical differences were evaluated by Student's *t*-test (between two groups) and one-way analysis of variance (ANOVA) with Tukey's *post-hoc* multiple comparisons test (among three groups) using GraphPad Prism 5 (GraphPad Software Inc.). The differences were considered statistically significant at $\alpha = 0.05$.

3. Results

3.1. Fabrication and characterization of a mineralized/unmineralized bilayer architecture with hierarchical nanostructures

A periodontium-like biphasic scaffold was fabricated in two steps: biomimetic self-assembly of collagen fibrils and nanohydroxyapatites to form a porous IMC scaffold, followed by microstamping of CGF arrays on the surface of interconnected IMC scaffolds and transformation into parallel-aligned fibrils after coagulation (Fig. 1a, Fig. S1, S2). To improve the compatibility between the IMC and CGF phases, collagen at 1:2 v/v ratio was mixed with CGF during the microstamping process to suppress phase separation. The collagen-reinforced CGF fibrils further improved the stability in aqueous solution (Fig. S3). Energy dispersive X-ray spectroscopy (EDS) demonstrated the element content of CGF was mainly composed of organic C, O and N, indicating unmineralized fibrils; whereas IMC mainly contained organic C, O and N, and inorganic Ca and P (Ca/P = 1.53), indicating mineralized collagen (Figs. S4a and b). The mineral content in IMC was further determined by TGA/DSC (Figs. S5b and c). The results showed that the residual mass of IMC and pure collagen was 44.86% and 27.69% respectively. The similar DSC curves of IMC and pure collagen indicated that collagen degradation occurred in IMC, and the mineral proportion of IMC was calculated as about 17.17%. Chemical composition analysis revealed that both CGF and IMC presented strong amide I, II, and III peaks. A symmetric $PO2^{-}$

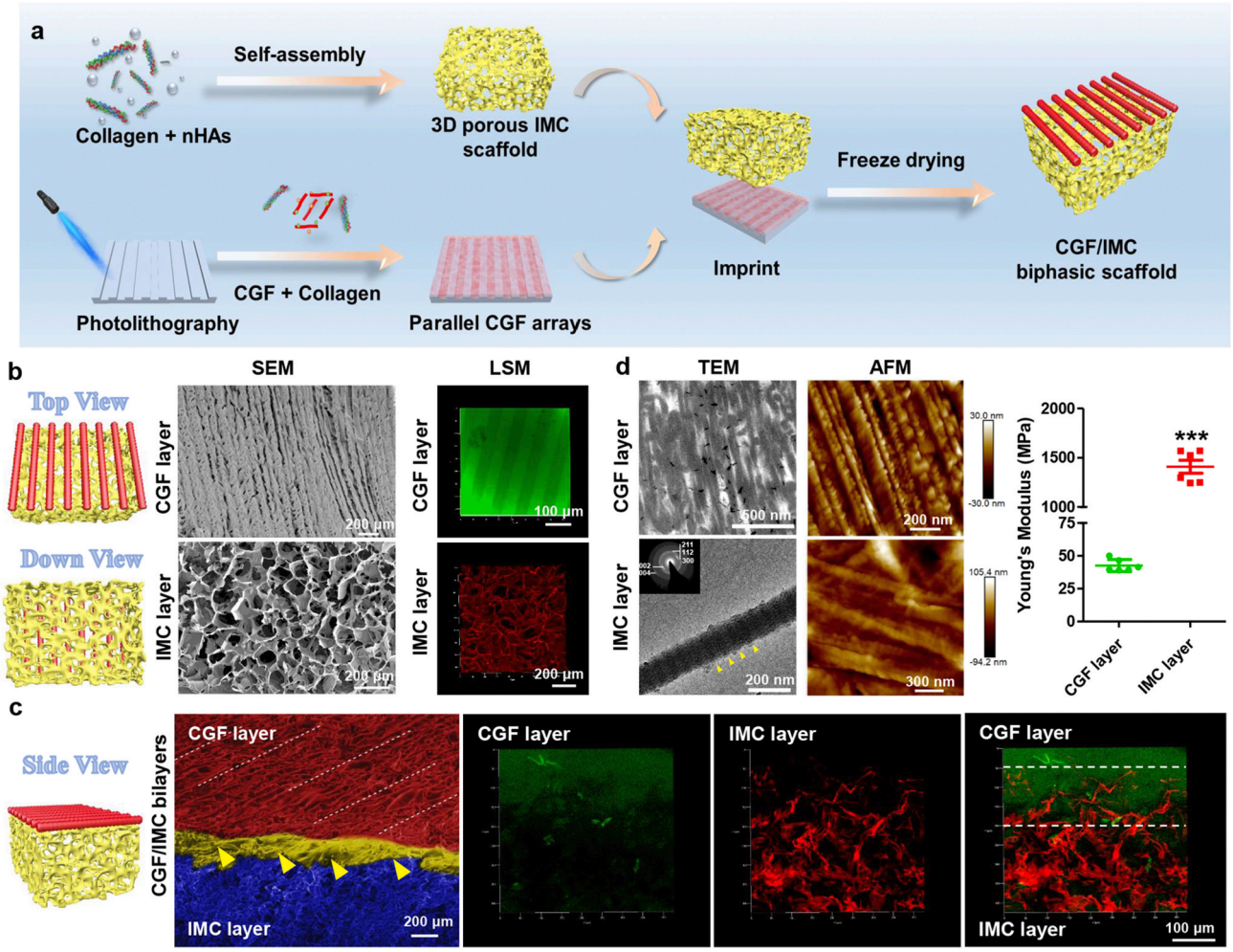

Fig. 1. Fabrication and characterization of a mineralized/unmineralized bilayer architecture. a) Schematic illustration for fabrication of hierarchical CGF/IMC biphasic scaffolds. b) SEM and LSM images of the CGF layer and the IMC layer in top-down view. c) SEM and LSM images of the interface of hierarchical CGF/IMC bilayers in side view. Yellow open arrowheads and white dot lines indicate interface of CGF/IMC (~150 μm). d) TEM and AFM nanostructures, and Young's modulus of the CGF layer and the IMC layer. CGF fibrils are parallel-aligned and IMC possesses typical D-periods (~67 nm, between two yellow open arrowheads). Selected area electron diffraction shows that the nano-hydroxyapatites in IMC exhibit a perfect crystalline structure, with *c*-axes preferentially orienting along the collagen axis (inset). ***: $P < 0.001$.

stretching band at 1092 cm^{-1} appeared in the CGF layer, ascribing to the phospholipids in the platelet membrane [26]. Obvious bands at 1030 cm^{-1}, 600 cm^{-1}, and 560 cm^{-1} appeared in the IMC layer, showing the presence of apatitic phosphate (Figs. S4c and d).

In top view, the unmineralized CGF layer exhibited a periodic parallel arrangement similar to the structure of periodontal ligament with a gap width of 50 μm; and the IMC layer possessed highly interconnected and uniform pores (153.7 ± 8.8 μm in diameter), as shown by SEM (Fig. 1b). In addition, the immunofluorescence results also indicated that the CGF layer had a parallel alignment with a uniform gap width of 50 μm, and the IMC layer had interconnected and uniform pores, similar to the SEM observations (Fig. 1b). Cross-sectional images showed a clear and well-defined interface between the two layers. The addition of collagen to the CGF phase improved compatibility with IMC, and the edge of the coagulated CGF fibrils penetrated the surface of the IMC scaffold such that mechanical interlocking and cohesion could be observed in side view (Fig. 1c, Fig. S1c). To further confirm whether the mineralized/unmineralized bilayers could successfully simulate the periodontal soft/hard tissue, TEM and AFM were applied to determine the hierarchical nanostructures and mechanical properties of each single phase. The results (Fig. 1d) showed that the CGF layer, with parallel-aligned fibrils (79.92 ± 19.35 nm), had a much lower Young's modulus of 42.62 ± 4.58 MPa, similar to that of natural periodontal ligament [27]. By contrast, the IMC layer, with the typical D-periods and nano-hydroxyapatites mainly depositing inside the collagenous gap regions [14], had a much higher Young's modulus of 1409.00 ± 160.83 MPa, similar to that of natural alveolar bone (Fig. 1d, Fig. S5a) [28]. By applying 50 cycles of uniaxial compression in wet conditions, compressive stress-strain curve was obtained for 3D CGF/IMC and elastic modulus was calculated as 137.60 ± 54.13 KPa (Fig. S4e), similar to that of 3D IMC [18].

3.2. *The growth factor-rich microenvironment of the CGF/IMC bilayer architecture*

To investigate whether the mineralized/unmineralized bilayers could effectively construct different growth factor microenvironments to initiate periodontal soft and hard tissue regeneration, immunofluorescent staining of the CGF layer and cross-sections of the CGF/IMC bilayers was performed to detect growth factors in the CGF/IMC bilayers. The results showed that TGF-β1 and VEGF were highly expressed in the CGF layer and at the interface of the two phases, with almost no expression in the IMC layer (Fig. 2a). CGF also contained a high level of PDGF-BB (Fig. S1a). To further investigate the sustained and controlled

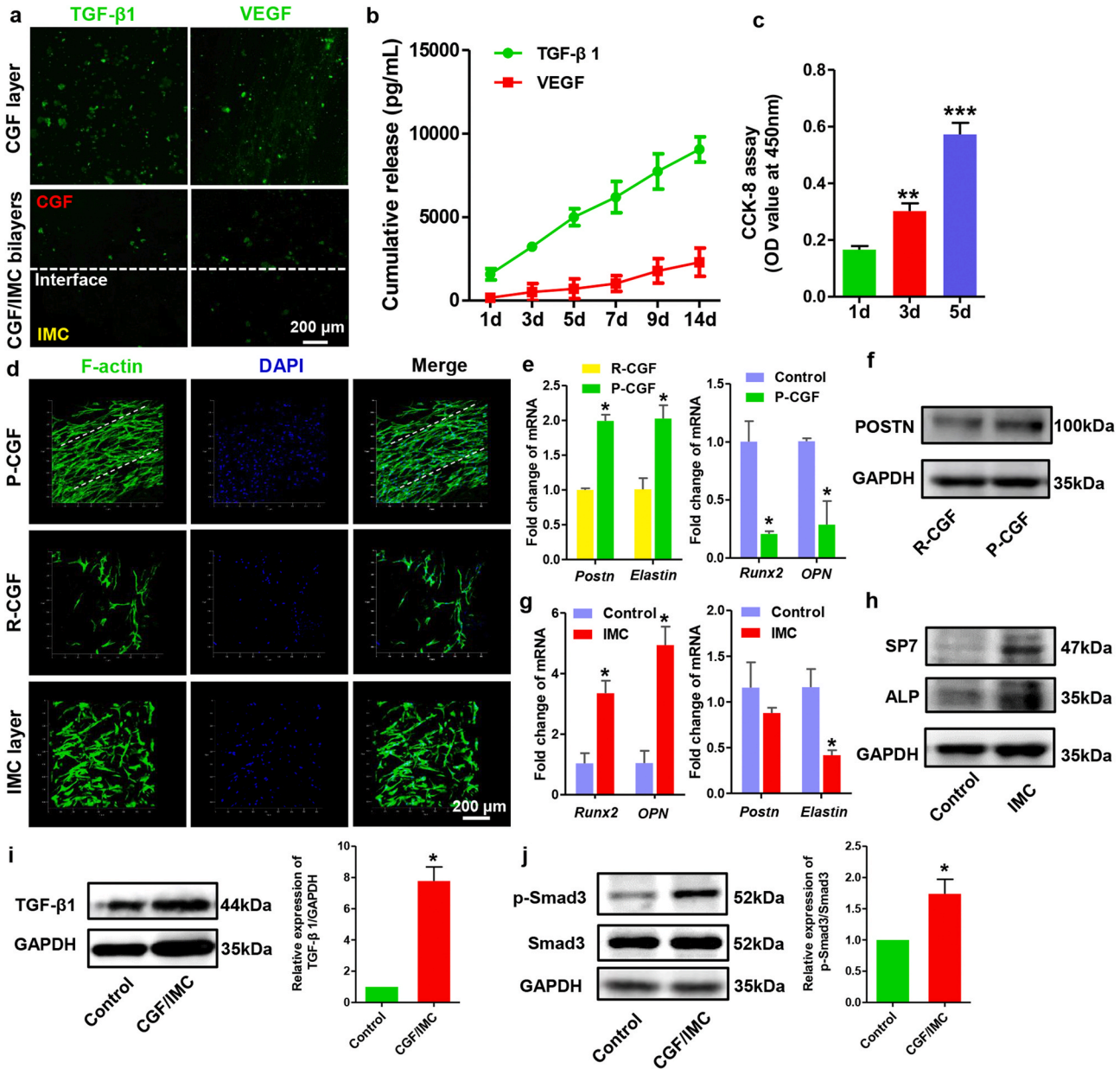

Fig. 2. Growth factor-rich microenvironment and cell regulation of the hierarchical CGF/IMC bilayer architecture *in vitro*. a) Immunofluorescent staining of TGF-β1 and VEGF in the CGF layer and cross-sections of the CGF/IMC bilayers. b) *In vitro* cumulative release of TGF-β1 and VEGF from the CGF/IMC bilayers for 14 days. c) CCK-8 assay. d) Cell arrangement in the parallel-arranged CGF (P-CGF), random-arranged CGF (R-CGF) and IMC layers at 1 day. e) mRNA expression levels of fibrogenic differentiation-related genes (*Postn* and *elastin*) in PDLSCs cultured on P-CGF and R-CGF at 7 days, and osteogenic differentiation-related genes (*Runx2* and *OPN*) in PDLSCs cultured on 6-well plate (Control) and P-CGF at 14 days. f) Western blotting of POSTN in P-CGF and R-CGF at 7 days. g) mRNA expression levels of osteogenic differentiation-related genes (*Runx2* and *OPN*) in PDLSCs cultured on 6-well plate and IMC at 14 days, and fibrogenic differentiation-related genes (*Postn* and *elastin*) in PDLSCs cultured on 6-well plate and IMC at 7 days. h) Western blotting of SP7 and ALP in PDLSCs cultured on 6-well plate and IMC at 7 days. i, j) Western blotting of TGF-β1, Smad3 and p-Smad3 in PDLSCs cultured on 6-well plate and CGF/IMC at 3 days. *: $P < 0.05$; **: $P < 0.01$; ***: $P < 0.001$.

release of growth factors by collagen-reinforced CGF fibrils, the supernatant was collected at different times (1, 3, 5, 7, 9, and 14 days), and quantitative analyses were performed using enzyme-linked immunosorbent assay kits. The *in vitro* cumulative release rate curve showed that TGF-β1 and VEGF could be released continuously for 14 days with the slow disintegration of CGF fibrils (Fig. 2b) [29]. CCK-8 assay indicated the good biocompatibility of the CGF/IMC bilayer scaffold, which promoted PDLSC proliferation with more than three times from day 1 to day 5 (Fig. 2c).

3.3. Cell regulation with the hierarchical CGF/IMC bilayer architecture in vitro

To verify the respective biological effects between the CGF phase and IMC phase, the binary scaffold was divided into monophasic, two-dimensional slices, and identified human PDLSCs (Fig. S6) were seeded separately onto CGF and IMC slices to investigate cell behaviors. The biological benefits of the parallel-arranged superstructure in the CGF layer were taken into consideration, and a disordered layer with random deposition of CGF fibrils was fabricated as a control. Compared with randomly arranged CGF, parallel CGF fibrils could attract more PDLSCs to form a fibroblast-like morphology with an oriented

arrangement in 1 day (Fig. 2d). Quantitative RT-PCR showed that the relative mRNA expression levels of two fibrogenic differentiation-related genes, *periostin* (*Postn*) and *elastin*, were significantly upregulated in the parallel-aligned CGF group after 7 days of incubation (Fig. 2e). Moreover, parallel-aligned CGF increased the protein expression level of POSTN after 7 days of incubation as revealed by Western blotting (Fig. 2f). By contrast, two osteogenic differentiation-related genes, *runt-related transcription factor 2* (*Runx2*) and *osteopontin* (*OPN*), were not highly expressed in the parallel-aligned CGF group. Interestingly, the interconnected IMC layer could trap PDLSCs with cross-arrangement through a porous structure (Fig. 2d). In the IMC layer, the osteogenic differentiation-related genes, *Runx2* and *OPN*, were significantly upregulated in human PDLSCs after 14 days of incubation (Fig. 2g), whereas the expression levels of fibrogenic differentiation-related genes (*Postn* and *elastin*) were relatively low. Western blotting further confirmed the promoting effect of IMC on osteogenic differentiation, with enhanced expression of early osteogenic differentiation-related proteins SP7 and ALP in human PDLSCs after 7 days of incubation (Fig. 2h).

To uncover the potential mechanism underlying the CGF/IMC biphasic scaffold, TGF-β1, as an important factor for PDLSC proliferation and periodontal maintenance and regeneration [30], was detected by Western blotting (Fig. 2i). It was shown that the protein expression level of TGF-β1, were significantly upregulated in human PDLSCs cultured on

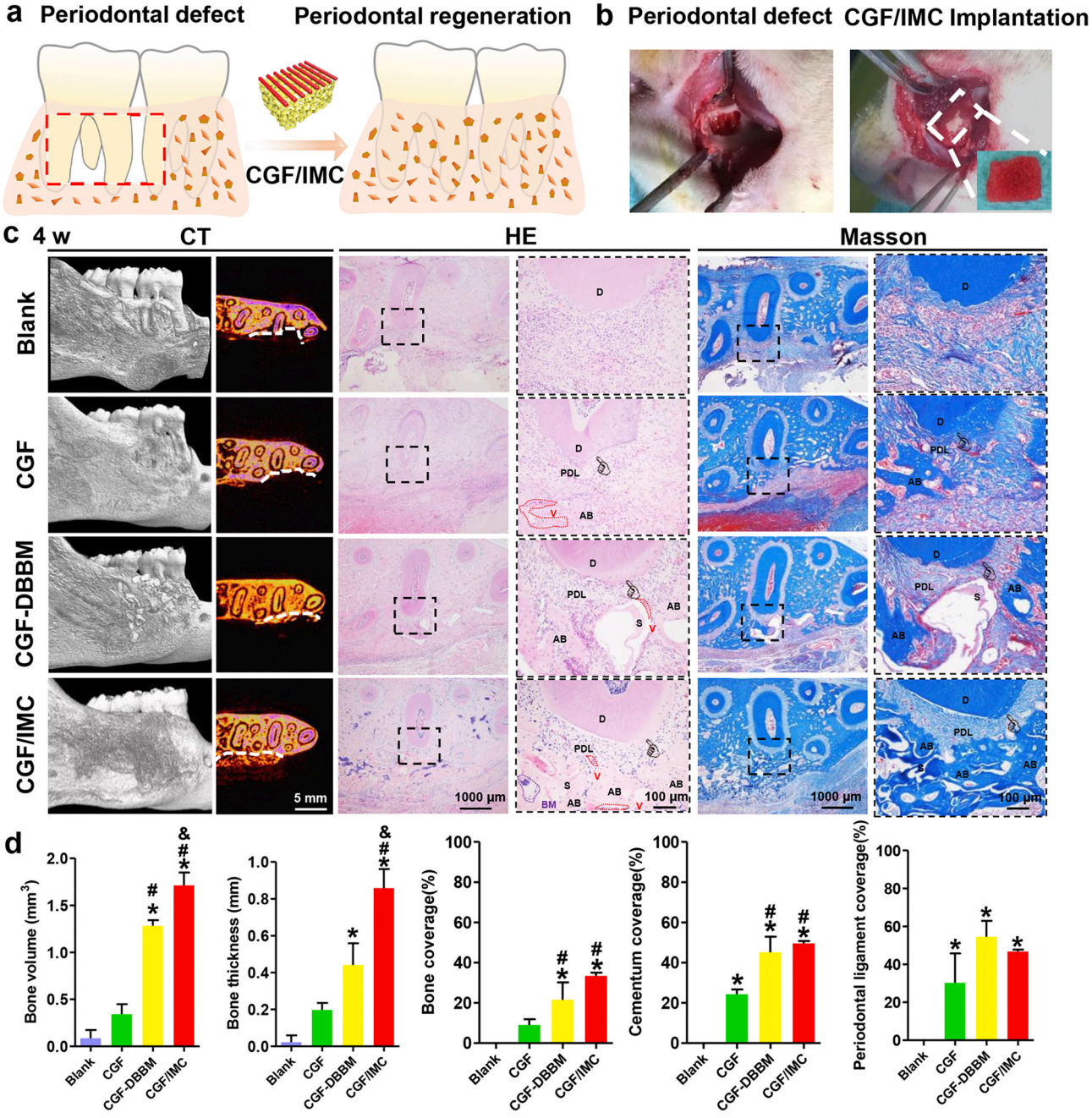

Fig. 3. *In situ* multilineage differentiation of the CGF/IMC bilayer architecture. a) Scheme of the transplantation of the CGF/IMC bilayer into rat periodontal tissue defects. b) Surgical images of periodontal defects and the CGF/IMC bilayer implantation. c) Micro-CT, HE and Masson's trichrome staining of cross-sections of periodontal defect repair at 4 weeks. White line indicates defect boundary in micro-CT images. D: dentin, PDL: periodontal ligament, AB: alveolar bone, S: scaffold, BM: bone marrow, V: vessel. d) Semi-quantitative analysis of newly formed alveolar bone, cementum and periodontal ligament percentage in micro-CT and HE images. *: $P < 0.05$ *versus* Blank, #: $P < 0.05$ *versus* CGF, &: $P < 0.05$ *versus* CGF–DBBM.

CGF/IMC for 3 days. The phosphorylation and expression of Smad3, downstream of the TGF-β1 signaling pathway, were also elevated in PDLSCs on day 3 (Fig. 2j). Similarly, Gu *et al.* showed TAZ promoted human PDLSC osteogenic differentiation via the Smad3 [31]. These findings demonstrated the activation of TGF-β1/Smad3 pathway by CGF/IMC.

3.4. *In situ* multilineage differentiation of the CGF/IMC bilayer architecture

To investigate the multilineage differentiation of the CGF/IMC biphasic scaffold *in vivo*, a rat maxillary complete periodontal defect model (with a 5 mm × 4 mm × 1 mm-sized defect) was established (Fig. 3a, b). Surgical photographs and micro-computed tomography (micro-CT) images showed that the periodontal tissue of the first molar, including alveolar bone, periodontal ligament, and cementum, was completely removed (Fig. S7). Rats treated with a monophasic CGF scaffold (CGF) or a non-hierarchical mechanical mixture of CGF and deproteinized bovine bone mineral (CGF–DBBM) were considered as controls; and the rat self-healing model was defined as the Blank group. At 4 weeks after implantation, micro-CT results (Fig. 3c) showed that relatively continuous and intact newly formed bone in the periodontal defect area was observed in the CGF/IMC group. In the controls, only a small amount of new bone was formed in the CGF–DBBM and CGF

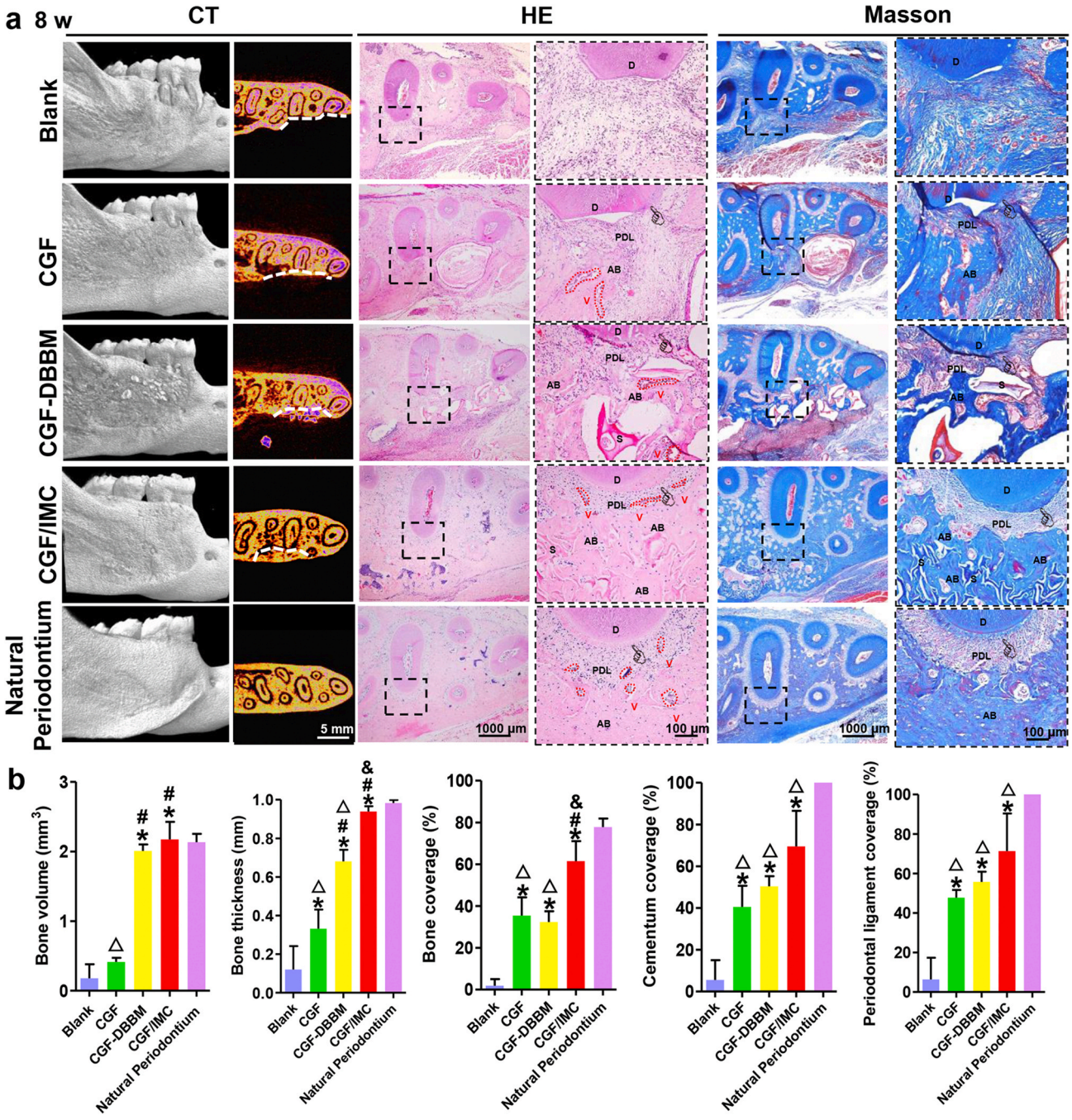

Fig. 4. Complete periodontal tissue regeneration *in vivo*. a) Micro-CT, HE and Masson's trichrome staining of periodontal tissue regeneration areas. White line displays defect boundary. D: dentin, PDL: periodontal ligament, AB: alveolar bone, S: scaffold, V: vessel, pointer: cementum. b) Semi-quantitative analysis of newly formed alveolar bone, cementum and periodontal ligament percentage in micro-CT and HE images. *: $P < 0.05$ *versus* Blank, #: $P < 0.05$ *versus* CGF, &: $P < 0.05$ *versus* CGF–DBBM, △: $P < 0.05$ *versus* Natural periodontium.

groups. As expected, there was almost no new alveolar bone in the Blank group, indicating that the rats did not have periodontal tissue self-regeneration ability. The results shown in Fig. 3d indicated that the bone volume and mean thickness of newly formed alveolar bone were significantly greater in the CGF/IMC group than in the other groups. Images of HE- and Masson's trichrome-stained tissues (Fig. 3c) revealed the formation of hierarchically staggered periodontal tissues, including neo-alveolar bone, neo-cementum, and neo-periodontal ligament, only in the CGF/IMC group, whereas little new-born periodontal-like soft/hard tissue was observed in the CGF and CGF–DBBM groups, and disordered connective tissue without cementum, periodontal ligament, or alveolar bone was observed in the Blank group. The above results indicate that only the CGF/IMC biphasic architecture could successfully induce stem cell multilineage differentiation into soft and hard periodontal tissues, which was similar to cell regulation results *in vitro*.

3.5. Complete periodontal tissue regeneration in vivo

To further achieve complete periodontal tissue regeneration, the implantation time was extended to 8 weeks. The micro-CT results showed that the newly formed alveolar bone in the CGF/IMC group was similar to natural alveolar bone, without an obvious boundary between the defect area and tooth area (Fig. 4a). In marked contrast, abundant low-density new bone and high-density undegraded materials were observed in the CGF–DBBM group, and only a small amount of relatively thin and continuous bone was seen in the CGF group. As expected, there was almost no new alveolar bone in the Blank group. The bone volume of new alveolar bone in the CGF/IMC group (2.173 ± 0.254 mm^3) was similar to that of native periodontium (2.135 ± 0.119 mm^3) and higher than those in the CGF–DBBM (2.010 ± 0.092 mm^3), CGF (0.414 ± 0.058 mm^3), and Blank groups (0.178 ± 0.203 mm^3) (Fig. 4b). The average thickness of new alveolar bone in the CGF/IMC group (0.939 ± 0.027 mm) was similar to that of native periodontium (0.983 ± 0.015 mm) and significantly greater than those in the CGF–DBBM (0.681 ± 0.060 mm), CGF (0.331 ± 0.100 mm), and Blank (0.121 ± 0.121 mm) groups. These results indicate complete regeneration of the alveolar bone could be achieved through CGF/IMC treatment. The microstructure of the regenerated periodontal tissues after 8 weeks was further investigated using HE and Masson's trichrome stainings (Fig. 4a). Newly formed functional periodontal tissues in the CGF/IMC group were composed mostly of alveolar bone, ligament fibers, cementum, and small amounts of incompletely degraded scaffold, and the tissue organization was highly similar to that of natural periodontium. Although certain amounts of alveolar bone, cementum, and periodontal ligament structures were also observed in the CGF–DBBM group, the regenerated tissue contained large numbers of discontinuous microstructures separated by undegraded, powdery materials. Non-mineralized tissue accounted for the majority of tissues observed in the CGF group, and there was almost no bone formation in the Blank group. As shown in Fig. 4b, the amount of new alveolar bone in the distal root defect region of the first molar in the CGF/IMC group ($61.49\% \pm 7.39\%$) was significantly greater than those in the CGF–DBBM ($32.37\% \pm 5.14\%$), CGF ($35.41\% \pm 8.75\%$), and Blank ($1.84\% \pm 3.19\%$) groups. The trend for newly formed cementum was consistent with that for alveolar bone. With regard to regenerated soft tissue, more new periodontal ligament ($71.29\% \pm 19.12\%$) was observed in the CGF/IMC group than in the CGF-DBBM ($55.72\% \pm 5.23\%$), CGF ($47.77\% \pm 3.89\%$), and Blank ($6.34\% \pm 10.99\%$) groups. The above results indicate that the CGF/IMC biphasic scaffold possesses complete periodontal tissue regeneration capacity, including that for mineralized and non-mineralized tissues.

3.6. Promotion of periodontal tissue regeneration by the CGF/IMC bilayer architecture by host stem cell recruitment and Smad3 activation

To better understand the mechanisms underlying the promotion of periodontal regeneration by biomimetic biphasic scaffolds, host mesenchymal stem cell (MSC) recruitment and molecular pathways were further examined using immunofluorescent and immunohistochemical stainings (Fig. 5). Two MSC-related markers, CD105 and CD90, were highly expressed in the periodontal defects in the CGF/IMC group at 4 weeks after transplantation (Fig. 5a, b). By contrast, only a low level of expression was detected in the CGF–DBBM group, and almost no expression of CD105, or CD90 was observed in the CGF and Blank groups. After 8 weeks implantation, the newly formed periodontal tissues in the CGF/IMC group contained the highest proportion of BMP2-positive cells (44.25 ± 5.25 per slice), whereas the protein expression levels were lower in the CGF–DBBM (13.67 ± 3.21 per slice) and CGF group (7.67 ± 2.52 per slice) (Fig. 5c, d). Moreover, the proportion of osteocalcin (OCN)-positive cells in the CGF/IMC group (75.67 ± 6.66 per slice) was also much higher than those in the CGF–DBBM (18.33 ± 4.93 per slice) and CGF (9.33 ± 6.03 per slice) groups. These results indicate that CGF/IMC promoted bone formation via elevating the expression of BMP2 and OCN. The periodontal ligament fiber marker, collagen-1 (COL-1), was highly expressed in the CGF/IMC (62.33 ± 7.02 per slice), CGF–DBBM (61.33 ± 10.26 per slice), and CGF (78.00 ± 3.46 per slice) groups, suggesting that large amounts of collagen were formed in all three groups. However, the expression of vascular endothelial growth factor receptor-1 (VEGFR-1), a marker of angiogenesis, was quite different among the three groups, with high expression in the CGF/IMC group (70.33 ± 11.68 per slice) but weaker expression in the CGF–DBBM (37.00 ± 6.08 per slice) and CGF groups (13.00 ± 2.65 per slice).

Further, we investigated whether the TGF-β1 pathway plays an important role in promoting periodontal hard/soft tissue regeneration. Immunofluorescent staining (Fig. 5a, b) showed that TGF-β1 was highly expressed in the periodontal defects in the CGF/IMC group, whereas only a low level of expression was detected in the CGF–DBBM group, and almost no expression was observed in the CGF and Blank groups after 4 weeks implantation. After 8 weeks implantation, TGF-β1 and Smad3 were examined in both new alveolar bone and periodontal ligament areas (Fig. 5c, d). In the periodontal ligament area, TGF-β1 was more highly expressed in the CGF/IMC group (204.00 ± 12.77 per slice) than in the CGF–DBBM (111.00 ± 8.54 per slice) and CGF (64.00 ± 10.58 per slice) groups. In the alveolar bone area, much higher expression of TGF-β1 (122.33 ± 16.62 per slice) was observed in the CGF/IMC group than in the CGF–DBBM (60.00 ± 6.00 per slice) and CGF (20.50 ± 3.54 per slice) groups. The trend in Smad3 expression was consistent with that for TGF-β1. Higher Smad3 expression in the periodontal ligament area was observed in the CGF/IMC group (202.33 ± 16.50 per slice) compared with the CGF-DBBM (88.33 ± 4.51 per slice) and CGF (71.67 ± 8.50 per slice) groups. The number of Smad3-positive cells in the alveolar bone region was also significantly higher in the CGF/IMC group (129.00 ± 5.29 per slice) than in the CGF–DBBM (52.66 ± 7.51 per slice) and CGF (9.00 ± 1.41 per slice) groups. These observations were consistent with the *in vitro* results, and suggested that the TGF-β1/Smad3 pathway could be activated during periodontal hard and soft tissue regeneration by CGF/IMC.

3.7. Host MSC recruitment and multilineage differentiation of the CGF/IMC bilayer architecture in an ectopic regeneration model

To further eliminate the influence of immune responses and confirm the potently functional role of the CGF/IMC biphasic scaffold in the recruitment and multilineage differentiation of host MSCs, an 8-week model of subcutaneous ectopic regeneration was established using immunodeficient mice. Micro-CT, SEM, and histological analyses were performed to examine the osteogenesis, fibrogenesis, and angiogenesis potential and stem cell recruitment capability of the CGF/IMC biphasic scaffold (Fig. 6a–d, Fig. S8). Mature bone island structures with abundant blood vessels formed in the CGF/IMC group, and some periodontal ligament fiber-like tissues were observed surrounding the new bone region accompanied by small amounts of undegraded materials. By

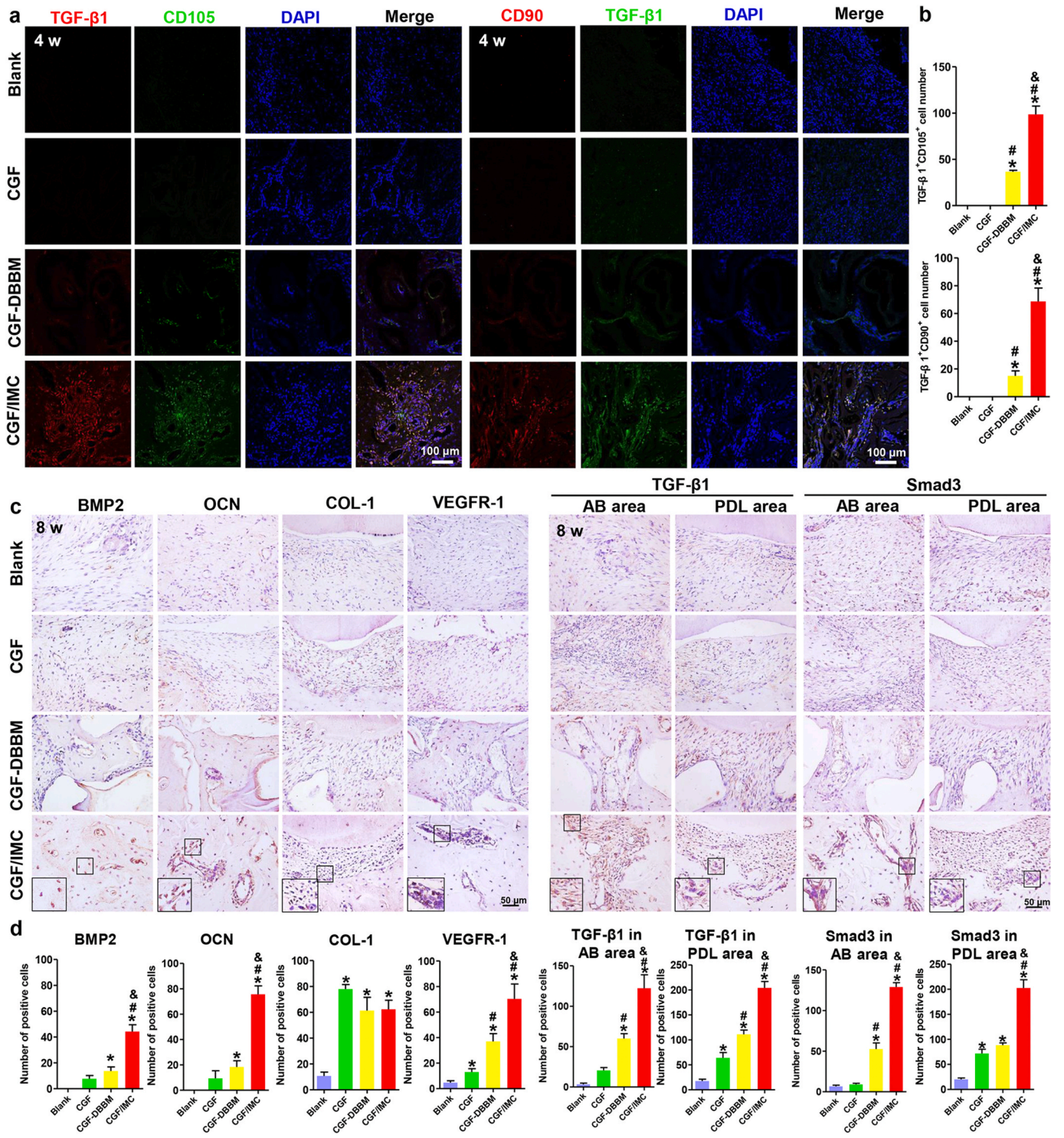

Fig. 5. Promotion of periodontal tissue regeneration by the CGF/IMC bilayer architecture by host stem cell recruitment and Smad3 activation. a) Immunofluorescent co-staining of TGF-β1 and CD105, and TGF-β1 and CD90 after 4 weeks implantation. b) Semi-quantitative analysis of positive cell numbers per slice of (a). c) Immunohistochemical staining of BMP2, OCN, COL-1, VEGFR-1, TGF-β1 and Smad3 in newly formed alveolar bone (AB) area and periodontal ligament (PDL) area after 8 weeks implantation. d) Semi-quantitative analysis of positive cell numbers per slice of (c). *: $P < 0.05$ *versus* Blank, #: $P < 0.05$ *versus* CGF, &: $P < 0.05$ *versus* CGF–DBBM.

contrast, the new bone in the CGF–DBBM group was immature and surrounded by muscle fibers (Fig. 6a, b, Fig. S8). Meanwhile, SEM images revealed collagen fiber-like structures and cells extending pseudopodia in the CGF/IMC group, with irregularly arranged bone-like structures found in the CGF–DBBM group. The results of immunohistochemical staining (Fig. 6c, d) showed that CD146$^+$ and STRO-1$^+$ MSCs were more abundant and more uniformly distributed in the CGF/IMC group (151.33 ± 26.84 and 130.00 ± 15.39, respectively) compared to the CGF–DBBM group (56.00 ± 4.58 and 45.33 ± 2.08, respectively), indicating that the CGF/IMC biphasic scaffold recruited more host CD146$^+$ and STRO-1$^+$ MSCs. Moreover, BMP2$^+$ (118.67 ± 8.14), COL-1$^+$ (68.00 ± 7.55), and VEGFR-1$^+$ (104.67 ± 11.68) cells were more

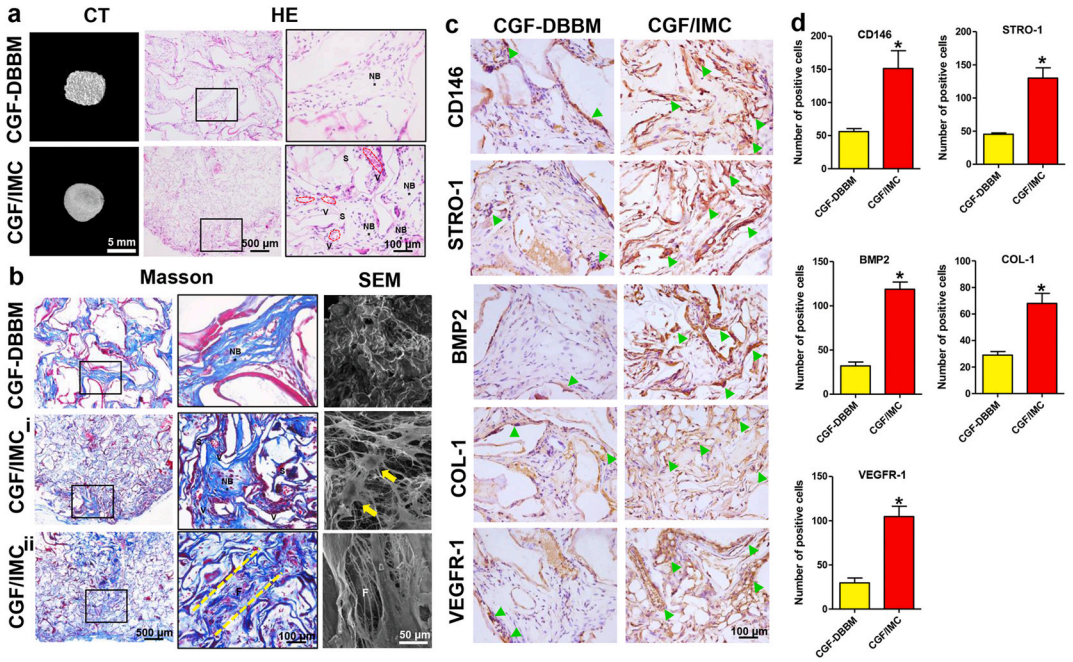

Fig. 6. Host MSC recruitment and multilineage differentiation of the CGF/IMC bilayer architecture in an ectopic regeneration model. a) Representative micro-CT images and HE staining images of neo-tissues. NB: new bone, S: scaffold, V: vessel. b) Representative Masson's trichrome staining and SEM images of neo-tissues. i) Bone-like tissue area; ii) PDL-like tissue area. F: fibers; Yellow arrows: cells with extending pseudopodia. c) Immunohistochemical staining of CD146, STRO-1, BMP2, COL-1 and VEGFR-1. Open arrowheads: positive cells. d) Semi-quantitative analysis of positive cell numbers per slice of (c). *: $P < 0.05$.

abundant in the CGF/IMC group than in the CGF–DBBM group (32.00 ± 4.36, 29.00 ± 2.65, 29.67 ± 5.51, respectively), indicating that the CGF/IMC biphasic scaffold itself exhibited osteogenic, fibrogenic, and angiogenic potential.

4. Discussion

The native periodontium is a complex and hierarchical organ, with mineralized, porous alveolar bone and non-mineralized, parallel-aligned periodontal ligament. The simulation of such a hard/soft tissue interface to achieve tissue regeneration poses unique challenges due to compositional, topological, and mechanical differences between the different tissues [2,4]. Here, we used biomimetic self-assembly and microstamping techniques to fabricate a periodontium-like biphasic scaffold, consisting of the mineralized IMC layer (resembling bone and cementum) and the unmineralized collagenized-CGF layer arranged in parallel (mimicking periodontal ligament). To improve the compatibility between the IMC and CGF phases, collagen was mixed with CGF during the microstamping process to suppress phase separation, which prolonged the disintegration time of the fibril structure and achieved a stable and distinct diphase interface. The acquired CGF/IMC biphasic scaffold was very similar to natural periodontal tissues in terms of their micro/nano structure, mechanical properties and growth factor microenvironments. As shown by SEM, the unmineralized CGF layer exhibited a periodontal ligament-like periodic parallel arrangement superstructure, which facilitated the migration and orientation of endogenous stem cell, thus promoting the parallel alignment of newly formed collagen fibers. Simultaneously, the mineralized IMC layer presented a bone-like microstructure with highly interconnected and uniform pores, which was suitable for host stem cell migration and vascular ingrowth, thus allowing new bone formation. In addition to the micro/nano structure, the two phases of the CGF/IMC biphasic scaffold exhibited differential composition and mechanical properties to simulate periodontal soft/-hard tissues [27,28]. Furthermore, growth factors play crucial roles in the complex process of biological tissue regeneration, including regulating cellular activities, stimulating ECM formation and angiogenesis, and regulating cell pathways that govern wound healing [32,33]. Conventional biomaterials with a single growth factor environment are difficult to regulate cell multi-morphological and multilineage differentiation to achieve periodontal regeneration [4,5]. The prepared CGF/IMC scaffold created differentiated growth factor environments between the two phases through endogenous release and exogenous recruitment. TGF-β1 is a landmark pleiotropic growth factor in periodontal tissue regeneration due to its functional role in promoting angiogenesis, cell differentiation, and ECM synthesis [30,35,36,41]. In addition, VEGF is equally important in the regeneration of periodontal tissues, because with adequate vascularization, abundant nutrition can be supplied to, and metabolic waste discharged from, freshly transplanted tissue-engineered biomaterials. As CGF is a mixture of growth factors, rich in various endogenous growth factors, including TGF-β1, VEGF, PDGF-BB, IGF-1, and bFGF [20,29], therefore TGF-β1 and VEGF were highly expressed in the micropatterned CGF phase and IMC/CGF interface, with almost no expression in the IMC layer. It is worth noting that although the IMC layer itself cannot secrete growth factors, its osteoid microenvironment could recruit endogenous stem cells, and eventually form a growth factor-rich environment suitable for cell osteogenesis [17]. The growth factor environment was not transient, the sustained and controlled release of growth factors could be achieved through the slow disintegration of collagen-reinforced CGF fibrils. The *in vitro* cumulative release rate curve showed that TGF-β1 and VEGF could be released continuously for up to 14 days. The CGF/IMC biphasic scaffold realizes a full-scale simulation of periodontal tissue in the micro-nano structure, mechanical properties and growth factor environment, which could mobilize host stem cells of dental origin to initiate periodontal hard and soft tissue regeneration.

The CGF/IMC biphasic scaffold successfully induced bidirectional differentiation of PDLSCs into periodontal ligament/osteogenesis. After one day of co-cultivation, parallel-aligned CGF fibrils could guide parallel arrangement of PDLSCs to form a fibroblast-like morphology. The oriented migration of stem cells mainly due to the parallel-aligned superstructure with uniform gaps in the ordered micropatterned CGF substrate, which might offer an optimal space for actin cytoskeleton

reorganization and cell lineage differentiation [34]. In comparison, PDLSCs were sparsely and irregularly attached to the randomly arranged CGF substrate without any orientation. Interestingly, the IMC phase with interconnected porous structure could induce cross-arrangement of PDLSCs with highly branched osteocyte-like shapes. In addition to differences in cell morphology, mRNA and protein expression level provided more clues for stem cell differentiation. In the parallel-aligned CGF group, two fibrogenic differentiation-related genes (*Postn* and *elastin*) and one fibrogenic differentiation-related protein (POSTN) were significantly upregulated after 7 days incubation, and the expression level of two osteogenic differentiation-related genes (*Runx2* and *OPN*) were obviously reduced. The IMC group showed the opposite trend with high expression of *Runx2* and *OPN,* and downregulated *Postn* and *elastin.* Although CGF can also promote the proliferation and osteogenesis of PDLSCs in a dose-dependent manner [23], here, the CGF layer with ordered microstructures could only induce a periodontal ligament fiber-like arrangement and fibrogenic differentiation of PDLSCs. The above experiments confirmed that the differences in micro-nano structure, mechanical properties and factor environment determined the fate of stem cells.

Complete and functional periodontium regeneration requires a highly coordinated spatiotemporal repair response, involving osteogenesis and cementogenesis concomitant with functional periodontal ligament reattachment [4]. The CGF/IMC biphasic scaffolds were implanted in critical-sized complete periodontal tissue defects in two stages: implantation for 4 weeks to investigate the capability of host stem cell recruitment and multilineage differentiation in early stage *in vivo*, and 8 weeks to observe the ability to achieve complete and functional periodontal tissue regeneration *in vivo*. After 4 weeks implantation, only the CGF/IMC biphasic scaffold group showed high expression of CD 90 and CD 105 in the periodontal defects, revealing that the host stem cells were effectively recruited. The Micro-CT, HE and Masson's trichrome stainings results confirmed that the recruited cells could further achieve multilineage differentiation into soft and hard periodontal tissues. As control groups, the enrichment of growth factors alone (monophasic CGF scaffold) could hardly load host stem cells, and mainly promoted cell fibrogenic differentiation due to its poor mechanical property. Although the mechanical mixture of CGF–DBBM provided sufficient mechanical supports and growth factor-rich microenvironment, the non-hierarchical substrates interfered the directed reorganization of the actin cytoskeleton, which were not conducive to inducing the multilineage differentiation of stem cells. After extending the implantation time to 8 weeks, the CGF/IMC biphasic scaffold potently reconstructed complete and functional periodontium with the insertion of periodontal ligament fibers into newly formed cementum and alveolar bone. Although periodontal ligament restoration was achieved with CGF–DBBM and the monophasic CGF scaffold to a certain extent compared to the self-healing group, the new periodontal ligament could not functionally insert into neo-bone. The possible mechanisms underlying excellent regenerative properties of CGF/IMC were as follows: the parallel-aligned non-mineralized fibers and porous mineralized scaffold in the CGF/IMC bilayers provide a hierarchical, periodontal-like microenvironment for local stem cell attachment, migration, proliferation, and fibrogenesis/osteogenesis differentiation; and a controlled release of diverse growth factors in the CGF/IMC biphasic scaffold may contribute to forming a niche-mimicking microenvironment to initiate the complex process of host stem cell recruitment and multilineage differentiation. Importantly, the stability and interconnection between the ordered CGF phase and the IMC layer enabled the morphofunctional integration of hard/soft tissue interfaces. The high degree of stiffness of IMC could have provided sufficient mechanical support for the periodontal defects and allowed stem cells to migrate through the interconnected pores, which facilitated remodeling of the ECM to form new bone [18]. Furthermore, the biodegradation rate of IMC was similar to that of natural bone, resulting in ingrowth of newly formed bone into the scaffold [14–16]. By contrast, the large DBBM crystals exhibited poor biocompatibility. The slow degradation rate and lack of pore structure in CGF–DBBM were not conducive to the recruitment and differentiation of stem cells, resulting in incomplete periodontal regeneration. Due to the rapid degradation rate and low stiffness of monophasic CGF, the degree of hard tissue regeneration in the monophasic CGF group was low.

The TGF-β1 pathway activation controls myriad events, including cell proliferation, differentiation, migration, ECM remodeling, and collagen accumulation, which are important for periodontal defect repair [35–37,41]. TGF-β1 could induce Smad3 phosphorylation and downstream fibrogenesis gene expression, including *COL-1*, *Postn*, and *elastin*, and thereby promoting tissue fibrogenesis [38]. Moreover, TGF-β1 can induce β-catenin activation through signaling crosstalk, which is essential for the ligament-fibroblastic differentiation of PDLSCs [38,39]. In this work, CGF/IMC biphasic architecture provided a periodontal-specific microenvironment for host stem cell recruitment, after which the recruited cells were induced to secrete TGF-β1 and VEGF, and TGF-β1 activation was initiated [17]. TGF-β1 increased Smad3 phosphorylation and the expression of downstream genes involved in osteogenesis and angiogenesis, such as *BMP2*, *OCN*, and *VEGFR-1*, thus facilitating the formation of neo-bone with new blood vessels. Therefore, the osteogenesis, ligament fiber formation, and angiogenesis in periodontal tissue regeneration might be regulated by TGF-β1/Smad3 signaling pathway. In the process of material-mediated periodontal regeneration, the local immune environment and the host inflammatory response are also important factors that regulate the function of stem cells and affect the outcomes of tissue regeneration [40]. To eliminate the influence of local immune responses and confirm the potently functional role of the CGF/IMC biphasic scaffold, a model of subcutaneous ectopic regeneration based on immunodeficient mice was established. After 8 weeks implantation, the CGF/IMC biphasic scaffold also achieved the regeneration of periodontal tissue, confirming its own potential for osteogenic, fibrogenic, and angiogenic, as well as the stem cell recruitment capability.

5. Conclusion

In this study, a biomimetic tissue-specific functional architecture resembling hard (bone and cementum) and soft (periodontal ligament) tissues was constructed by integration of self-assembly and microstamping strategies. In the hierarchical biphasic architecture, the self-assembled porous IMC scaffold with higher Young's modulus exhibited osteogenic differentiation potential, whereas the micropatterned CGF fibers with lower Young's modulus exhibited fibrogenic differentiation potential. After implantation in critical-sized complete periodontal tissue defects, the biomimetic biphasic architecture potently reconstructed native periodontium with the insertion of periodontal ligament fibers into newly formed cementum and alveolar bone by recruiting host MSCs. The TGF-β1/Smad3 pathway played an important role in CGF/IMC-induced periodontal regeneration (Scheme 1). These findings will contribute to the advancement of regenerative therapies for complex tissue regeneration.

Declaration of competing interest

The authors declare no conflict of interests in this work.

CRediT authorship contribution statement

Min Yu: Conceptualization, Investigation, Methodology, Validation, Formal analysis, Data curation, Visualization, Writing – original draft. **Dan Luo:** Conceptualization, Methodology, Formal analysis, Visualization, Writing – original draft, Writing – review & editing. **Jing Qiao:** Investigation, Methodology, Validation, Resources, Data curation. **Jiusi Guo:** Visualization. **Danqing He:** Methodology, Validation. **Shanshan Jin:** Methodology, Validation, Formal analysis. **Lin Tang:** Formal

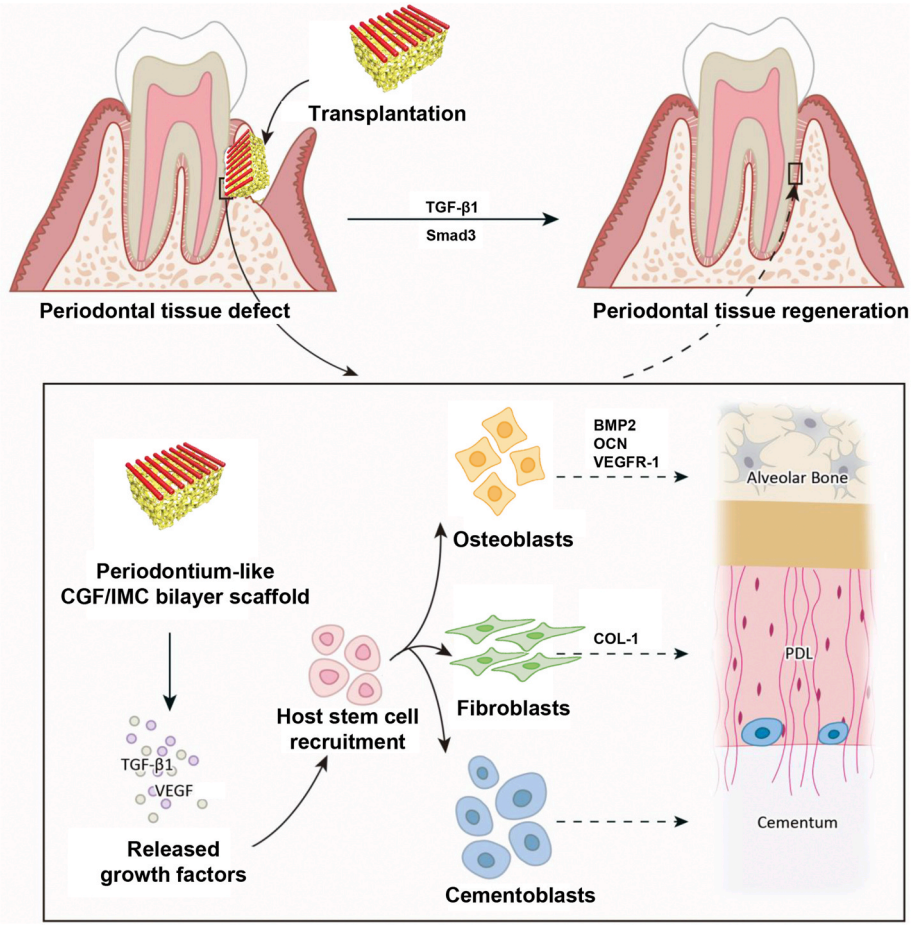

Scheme 1. Potential mechanisms of periodontal hard/soft tissue regeneration by the hierarchical CGF/IMC bilayer architecture.

analysis, Data curation, Visualization. **Yu Wang:** Methodology, Validation, Formal analysis, Data curation. **Xin Shi:** Visualization. **Jing Mao:** Methodology, Validation, Data curation. **Shengjie Cui:** Methodology, Formal analysis. **Yu Fu:** Validation, Formal analysis, Data curation. **Zixin Li:** Investigation, Formal analysis. **Dawei Liu:** Validation, Data curation. **Ting Zhang:** Investigation, Methodology. **Chi Zhang:** Methodology. **Zhou Li:** Supervision, Validation, Writing – review & editing. **Yongsheng Zhou:** Conceptualization, Validation, Resources, Writing – review & editing, Supervision, Project administration, Funding acquisition. **Yan Liu:** Conceptualization, Validation, Formal analysis, Resources, Data curation, Writing – review & editing, Supervision, Visualization, Project administration, Funding acquisition.

Acknowledgments

This work was supported by the National Natural Science Foundations of China No. 81871492 (Y.L.), No. 51902344 (D.L.) and No. 61875015 (Z.L.), Ten-Thousand Talents Program QNBJ2019-2 (Y.L.), Key R & D Plan of Ningxia Hui Autonomous Region No. 2020BCG01001 (Y.L.), National Key R&D Project from Minister of Science and Technology of China No. 2016YFA0202703 (D.L.).

Appendix A. Supplementary data

Supplementary data to this article can be found online at https://doi.org/10.1016/j.bioactmat.2021.08.024.

References

[1] B.L. Pihlstrom, B.S. Michalowicz, N.W. Johnson, Periodontal diseases, Lancet 366 (9499) (2005) 1809–1820.
[2] H.N. Woo, Y.J. Cho, S. Tarafder, C.H. Lee, The recent advances in scaffolds for integrated periodontal regeneration, Bioact Mater. 6 (10) (2021) 3328–3342.
[3] Y. Liang, X. Luan, X. Liu, Recent advances in periodontal regeneration: a biomaterial perspective, Bioact Mater. 5 (2) (2020) 297–308.
[4] C. Vaquette, S.P. Pilipchuk, P.M. Bartold, D.W. Hutmacher, W.V. Giannobile, S. Ivanovski, Tissue engineered constructs for periodontal regeneration: current status and future perspectives, Adv. Healthc. Mater. 7 (21) (2018) 1800457.
[5] J. Tan, M. Zhang, Z. Hai, C. Wu, J. Lin, W. Kuang, H. Tang, Y. Huang, X. Chen, G. Liang, Sustained release of two bioactive factors from supramolecular hydrogel promotes periodontal bone regeneration, ACS Nano 13 (5) (2019) 5616–5622.
[6] H. Cho, S. Tarafder, M. Fogge, K. Kao, C.H. Lee, Periodontal ligament stem/progenitor cells with protein-releasing scaffolds for cementum formation and integration on dentin surface, Connect. Tissue Res. 57 (6) (2016) 488–495.
[7] H. Dan, C. Vaquette, A.G. Fisher, S.M. Hamlet, Y. Xiao, D.W. Hutmacher, S. Ivanovski, The influence of cellular source on periodontal regeneration using calcium phosphate coated polycaprolactone scaffold supported cell sheets, Biomaterials 35 (1) (2014) 113–122.
[8] E.C. Carlo Reis, A.P. Borges, M.V. Araujo, V.C. Mendes, L. Guan, J.E. Davies, Periodontal regeneration using a bilayered PLGA/calcium phosphate construct, Biomaterials 32 (35) (2011) 9244–9253.
[9] C.H. Park, H.F. Rios, Q. Jin, M.E. Bland, C.L. Flanagan, S.J. Hollister, W. V. Giannobile, Biomimetic hybrid scaffolds for engineering human tooth-ligament interfaces, Biomaterials 31 (23) (2010) 5945–5952.
[10] S. Sowmya, U. Mony, P. Jayachandran, S. Reshma, R.A. Kumar, H. Arzate, S. V. Nair, R. Jayakumar, Tri-layered nanocomposite hydrogel scaffold for the concurrent regeneration of cementum, periodontal ligament, and alveolar bone, Adv. Healthc. Mater. 6 (7) (2017) 1601251.
[11] R. De Santis, A. Gloria, T. Russo, U. D'Amora, S. Zeppetelli, A. Tampieri, T. Herrmannsdorfer, L. Ambrosio, A route toward the development of 3D magnetic scaffolds with tailored mechanical and morphological properties for hard tissue regeneration: preliminary study, Virtual Phys. Prototyp. 6 (4) (2011) 189–195.
[12] S. Maietta, T. Russo, R. De Santis, D. Ronca, F. Riccardi, M. Catauro, M. Martorelli, A. Gloria, Further theoretical insight into the mechanical properties of

polycaprolactone loaded with organic-inorganic hybrid fillers, Materials 11 (2) (2018) 312.
[13] C.H. Park, H.F. Rios, Q. Jin, J.V. Sugai, M. Padial-Molina, A.D. Taut, C.L. Flanagan, S.J. Hollister, W.V. Giannobile, Tissue engineering bone-ligament complexes using fiber-guiding scaffolds, Biomaterials 33 (1) (2012) 137–145.
[14] Y. Liu, N. Li, Y.P. Qi, L. Dai, T.E. Bryan, J. Mao, D.H. Pashley, F.R. Tay, Intrafibrillar collagen mineralization produced by biomimetic hierarchical nanoapatite assembly, Adv. Mater. 23 (8) (2011) 975–980.
[15] Y. Liu, S. Liu, D. Luo, Z. Xue, X. Yang, L. Gu, Y.H. Zhou, T. Wang, Hierarchically staggered nanostructure of mineralized collagen as a bone-grafting scaffold, Adv. Mater. 28 (39) (2016) 8740–8748.
[16] Y. Liu, D. Luo, X.X. Kou, X.D. Wang, F.R. Tay, Y. Sha, Y.H. Gan, Y.H. Zhou, Hierarchical intrafibrillar nano-carbonated apatite assembly improves nanomechanics and cytocompatibility of mineralized collagen, Adv. Funct. Mater. 23 (11) (2013) 1404–1411.
[17] Y. Liu, D. Luo, M. Yu, Y. Wang, S.S. Jin, Z.X. Li, S.J. Cui, D.Q. He, T. Zhang, T. Wang, Y.H. Zhou, Thermodynamically controlled self-assembly of hierarchically staggered architecture as an osteoinductive alternative to bone autografts, Adv. Funct. Mater. 29 (10) (2019) 1806445.
[18] S.S. Jin, D.Q. He, D. Luo, Y. Wang, M. Yu, B. Guan, Y. Fu, Z.X. Li, T. Zhang, Y. H. Zhou, C.Y. Wang, Y. Liu, A biomimetic hierarchical nanointerface orchestrates macrophage polarization and mesenchymal stem cell recruitment to promote endogenous bone regeneration, ACS Nano 13 (6) (2019) 6581–6595.
[19] Y. Fu, S. Liu, S.J. Cui, X.X. Kou, X.D. Wang, X.M. Liu, Y. Sun, G.N. Wang, Y. Liu, Y. H. Zhou, Surface chemistry of nanoscale mineralized collagen regulates periodontal ligament stem cell fate, ACS Appl. Mater. Interfaces 8 (25) (2016) 15958–15966.
[20] L.F. Rodella, G. Favero, R. Boninsegna, B. Buffoli, M. Labanca, G. Scari, L. Sacco, T. Batani, R. Rezzani, Growth factors, CD34 positive cells, and fibrin network analysis in concentrated growth factors fraction, Microsc. Res. Tech. 74 (8) (2011) 772–777.
[21] F. Tabatabaei, Z. Aghamohammadi, L. Tayebi, *In vitro* and *in vivo* effects of concentrated growth factor on cells and tissues, J. Biomed. Mater. Res. A. 108 (6) (2020) 1338–1350.
[22] X. Li, H. Yang, Z. Zhang, Z. Yan, H. Lv, Y. Zhang, B. Wu, Concentrated growth factor exudate enhances the proliferation of human periodontal ligament cells in the presence of TNFalpha, Mol. Med. Rep. 19 (2) (2019) 943–950.
[23] B. Yu, Z. Wang, Effect of concentrated growth factors on beagle periodontal ligament stem cells *in vitro*, Mol. Med. Rep. 9 (1) (2014) 235–242.
[24] G. Intini, The use of platelet-rich plasma in bone reconstruction therapy, Biomaterials 30 (28) (2009) 4956–4966.
[25] Y. Wang, S.S. Jin, D. Luo, D.Q. He, C. Shi, L.S. Zhu, B. Guan, Z.X. Li, T. Zhang, Y. H. Zhou, C.Y. Wang, Y. Liu, Functional regeneration and repair of tendons using biomimetic scaffolds loaded with recombinant periostin, Nat. Commun. 12 (1) (2021) 1293.
[26] W. Hübner, H.H. Mantsch, Orientation of specifically 13C=O labeled phosphatidylcholine multilayers from polarized attenuated total reflection FT-IR spectroscopy, Biophys. J. 59 (6) (1991) 1261–1272.
[27] R.A. Reinhardt, Y.C. Pao, R.F. Krejci, Periodontal ligament stresses in the initiation of occlusal traumatism, J. Periodontal. Res. 19 (3) (1984) 238–246.
[28] T.J. Knaup, C. Dirk, S. Reimann, L. Keilig, M. Eschbach, H. Korbmacher-Steiner, C. Bourauel, Time-dependent behavior of porcine periodontal ligament: a combined experimental, numeric *in-vitro* study, Am. J. Orthod. 153 (1) (2018) 97–107.
[29] M. Yu, X. Wang, Y. Liu, J. Qiao, Cytokine release kinetics of concentrated growth factors in different scaffolds, Clin. Oral Invest. 23 (4) (2019) 1663–1671.
[30] H. Maeda, N. Wada, A. Tomokiyo, S. Monnouchi, A. Akamine, Prospective potency of TGF-β1 on maintenance and regeneration of periodontal tissue, Int. Rev. Cell Mol. Biol. 304 (2013) 283–367.
[31] K. Gu, X. Fu, H. Tian, Y. Zhang, A. Li, Y. Wang, Y. Wen, W. Gu, TAZ promotes the proliferation and osteogenic differentiation of human periodontal ligament stem cells via the p-SMAD3, J. Cell. Biochem. 121 (2) (2020) 1101–1113.
[32] A. Nanci, D.D. Bosshardt, Structure of periodontal tissues in health and disease, Periodontol 40 (2000) 11–28.
[33] E. Anitua, M. Sanchez, G. Orive, Potential of endogenous regenerative technology for in situ regenerative medicine, Adv. Drug Deliv. Rev. 62 (7–8) (2010) 741–752.
[34] W. Liu, Y. Wei, X. Zhang, M. Xu, X. Yang, X. Deng, Lower extent but similar rhythm of osteogenic behavior in hBMSCs cultured on nanofibrous scaffolds versus induced with osteogenic supplement, ACS Nano 7 (8) (2013) 6928–6938.
[35] K.K. Kim, D. Sheppard, H.A. Chapman, TGF-β1 signaling and tissue fibrosis, Cold Spring Harbor Perspect. Biol. 10 (4) (2018) a022293.
[36] X. Wang, F. Li, L. Xie, J. Crane, G. Zhen, Y. Mishina, R. Deng, B. Gao, H. Chen, S. Liu, P. Yang, M. Gao, M. Tu, Y. Wang, M. Wan, C. Fan, X. Cao, Inhibition of overactive TGF-β attenuates progression of heterotopic ossification in mice, Nat. Commun. 9 (1) (2018) 551.
[37] P. Wang, M.L. Luo, E. Song, Z. Zhou, T. Ma, J. Wang, N. Jia, G. Wang, S. Nie, Y. Liu, F. Hou, Long noncoding RNA lnc-TSI inhibits renal fibrogenesis by negatively regulating the TGF-β/Smad3 pathway, Sci. Transl. Med. 10 (462) (2018) 2039.
[38] X. Guo, X.F. Wang, Signaling cross-talk between TGF-beta/BMP and other pathways, Cell Res. 19 (1) (2009) 71–88.
[39] J.C. Lim, S.H. Bae, G. Lee, C.J. Ryu, Y.J. Jang, Activation of β-catenin by TGF-β1 promotes ligament-fibroblastic differentiation and inhibits cementoblastic differentiation of human periodontal ligament cells, Stem Cell. 38 (2020) 1612–1623.
[40] J. Liu, B. Chen, J. Bao, Y. Zhang, L. Lei, Macrophage polarization in periodontal ligament stem cells enhanced periodontal regeneration, Stem Cell Res. Ther. 10 (1) (2019) 320.
[41] T. Kawai, W. Katagiri, M. Osugi, Y. Sugimura, H. Hibi, M. Ueda, Secretomes from bone marrow-derived mesenchymal stromal cells enhance periodontal tissue regeneration, Cytotherapy 17 (4) (2015) 369–381.
[42] B.M. Seo, M. Miura, S. Gronthos, P.M. Bartold, S. Batouli, J. Brahim, M. Young, P. G. Robey, C.Y. Wang, S. Shi, Investigation of multipotent postnatal stem cells from human periodontal ligament, Lancet 364 (9429) (2004) 149–155.
[43] G.N. King, N. King, A.T. Cruchley, J.M. Wozney, F.J. Hughes, Recombinant human bone morphogenetic protein-2 promotes wound healing in rat periodontal fenestration defects, J. Dent. Res. 76 (8) (1997) 1460–1470.